RMetS
Royal Meteorological Society

Genesis of southwest vortices and its relation to Tibetan Plateau vortices

Lun Li,[a]* Renhe Zhang[b,c] and Min Wen[a]
[a]*State Key Laboratory of Severe Weather, Chinese Academy of Meteorological Sciences, Beijing, China*
[b]*Institute of Atmospheric Sciences, Fudan University, Shanghai, China*
[c]*CAS Center for Excellence in Tibetan Plateau Earth Sciences, Beijing, China*

*Correspondence to: L. Li, Chinese Academy of Meteorological Sciences, 46 Zhong-Guan-Cun South Avenue, Beijing, 100081, China. E-mail: lilun@camscma.cn

SWVs are important summer rain-producing systems over southwestern China, and even wider areas in eastern China when they move eastward. Based on the final analyses data (FNL) of the Global Forecasting System of the National Centers for Environment Prediction, the role played by Tibetan Plateau vortices (TPVs) in the genesis processes of vortices in southwest China, referred to as southwest vortices (SWVs) is investigated. Since the TPVs and SWVs are most active in summer, the cases in May–August are studied. It is revealed that the TPVs moving off the Tibetan Plateau (moving-off TPVs) can exert significant effects on the genesis of SWVs through both dynamic and thermodynamic processes. The moving-off TPVs are favourable for the generation of SWVs through strengthening the cyclonic vorticity, convergence and ascending motion. Diagnoses of the potential vorticity budgets reveal that the condensational latent heat has the greatest contribution to the generation of SWVs. Analysis of the water vapour budget indicates that the water vapour is mainly transported from south of the genesis region of SWVs associated with strong southerlies. It is demonstrated that the southerlies and associated water vapour transport are another prominent factor affecting the genesis of the SWVs.

Key Words: Tibetan Plateau vortices; southwest vortices; genesis process

Received 21 February 2017; Revised 20 June 2017; Accepted 23 June 2017; Published online in Wiley Online Library 7 August 2017

1. Introduction

Southwest vortices (SWVs) are mesoscale cyclonic circulations most clearly identified at 700 hPa occurring over southwestern China, such as over the eastern and southeastern flanks of the Tibetan Plateau (Figure 1). The horizontal scale is typically several hundred kilometres, and vertical scale is relatively shallow in the genesis stage, and much deeper (500 hPa and above) during the development process (Lu, 1986; Wang and Orlanski, 1987; Kuo *et al*., 1988; Wang *et al*., 1993; Qiao and Zhang, 1994; Li, 2002; Chen and He, 2008). Although the SWVs generate throughout the year, they are important summer rain-producing systems affecting the rainfall over southwestern China, and even wider areas in eastern China when they move eastward. A lot of flood disasters are closely related to the presence of SWVs (Tao, 1980; Lu, 1986; Chen *et al*., 2003). Therefore, study of the genesis mechanism of SWVs is important not only in understanding the SWVs themselves, but also in forecasting precipitation over southwestern and even eastern China.

Tibetan Plateau vortices (TPVs) are the major mesoscale rain-producing systems forming over the Tibetan Plateau defined at 500 hPa (Ye and Gao, 1979). Most of the TPVs originate in the period from June to August, and the maximum of occurrence frequency of TPVs appears in June. The typical spatial scales of TPVs are about 400–800 km in the horizontal and 2–3 km in the vertical (Ye and Gao, 1979; Lhasa Workgroup for Tibetan Plateau Meteorology Research, 1981; Luo, 1992; Luo *et al*., 1994). Most TPVs originate over the central-western plateau, and decay over the eastern plateau, especially over the sloping terrain at the eastern edge of the Tibetan Plateau (Ye and Gao, 1979; Wang *et al*., 2009). The occurrence of TPVs is mainly modulated by the 10–30 day intraseasonal oscillation (ISO) (Zhang *et al*., 2014). Some TPVs can be maintained for a long time and move eastward, off the plateau (Ye and Gao, 1979; Tao and Ding, 1981; Qiao and Zhang, 1994; Li, 2002). The vortices moving off the Tibetan Plateau to southwestern China (hereafter referred to as moving-off TPVs) often interact with SWVs located to the east of the Tibetan Plateau, triggering heavy rainfall (Kuo *et al*., 1986; Fu *et al*., 2011).

Previous studies (as detailed below) mainly focused on the relation between the moving-off TPVs and pre-existing SWVs as well as the rainfall induced by these two kinds of vortices. It has been revealed that when the TPVs are located to the west of 100°E over the Tibetan Plateau, the sinking airflow to the east of the TPVs will hinder the development of the SWVs, but the TPVs will be favourable for the development of SWVs when they are located

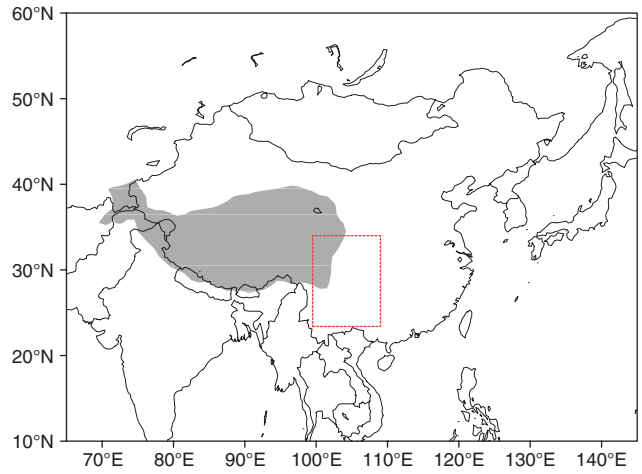

Figure 1. Position of the Tibetan Plateau (grey shading), and the scope of southwest China (red frame).

to the east of 100°E (Chen *et al*., 2004; Xiao *et al*., 2009; Zhou *et al*., 2009). Also, the TPVs have important effects on the genesis of the SWVs when they move off the plateau. In the effects of TPVs on the genesis of SWVs, Wang and Orlanski (1987) utilized a primitive equation model applied to a limited area with 17 layers, and showed that condensational latent heating associated with the precipitation over the eastern flank of the Tibetan Plateau plays the most important role, while some others highlighted the dynamic effects (e.g. horizontal winds and vertical motion) (Chen *et al*., 2004; Xiao *et al*., 2009; Zhou *et al*., 2009). Besides, Kuo *et al*. (1988) considered that the thermodynamic process (e.g. latent heating and surface energy flux) has little effect on the genesis of SWVs through numerical experiments based on a version of the Penn State University/National Center for Atmospheric Research (PSU/NCAR) mesoscale model. Therefore, how TPVs affect the genesis of SWVs is still unclear, and the contradictory results of Wang and Orlanski (1987) and Kuo *et al*. (1988) are from numerical models. We need to investigate the effect of TPVs on the genesis of SWVs through analysis of atmospheric reanalysis data.

As shown above, only a few studies discussed the effects of TPVs on the genesis of SWVs, but by considering just one case, and obtained contradictory results from numerical models. The present study will focus on the role played by TPVs in the genesis process of SWVs by analysis of atmospheric reanalysis data. We investigate the genesis mechanisms of SWVs by considering the moving-off TPVs (which we label Situation A). The mechanisms are further verified by comparison with situations of moving-off TPVs that are unaccompanied by the generation of SWVs (Situation B) and genesis process of SWVs without the moving-off TPVs (Situation C). Each situation includes nine cases, which is more comprehensive and solid than studies based on just one case.

In section 2, we describe the data and methods. Throughout sections 3–5 we consider Situation A, and then contrast Situations A, B and C in section 6. The features of large-scale circulations associated with SWVs in Situation A are shown in section 3. The dynamic and thermodynamic features in the genesis region of SWVs induced by the moving-off TPVs are discussed in section 4. In section 5, the genesis mechanism of SWVs in Situation A is investigated. By comparing Situation A with Situations B and C, the influence of TPVs is further discussed in section 6. Conclusions and discussion are given in section 7.

2. Data and method

2.1. Data

The circulation features, calculations of atmospheric apparent heat source (Q_1), apparent moisture sink (Q_2), as well as the potential vorticity (PV) budget in the present study are based on FNL (Final) Operational Global Analysis data with 6 h interval and $1^\circ \times 1^\circ$ horizontal resolution from the Global Forecasting System of the National Centers for Environmental Prediction (NCEP) (http://rda.ucar.edu/datasets/ds083.2, ds083.2—DOI: 10.5065/D6M043C6) for the period in May–August of 2000–2011. The rawinsonde data observed at 272 stations twice a day over China from May–August of 2000–2011 provided by the National Meteorological Information Center of the China Meteorological Administration is utilized to make sure that the FNL data can basically present the circulations associated with the observed vortices. In each case we compared the locations of the vortex observed by the rawinsonde data with those in FNL data. Although the observational stations are scarce over the western Tibetan Plateau, and the interval of the observational radiosonde data is 12 h, the locations of TPVs and SWVs over the central and eastern plateau from FNL data and the observational data are similar at the same time. The distance between the vortex centres derived from these two datasets in each case is less than 2° in both zonal and meridional directions (figure not shown). In fact, Li *et al*. (2014b) compared the occurrence frequency of Tibetan Plateau vortices in FNL data with that in observations and found that they are consistent, indicating the good capability of FNL data in representing Tibetan Plateau vortices.

2.2. Case selection

A TPV is defined as a low which forms over the Tibetan Plateau with closed contour lines or cyclonic winds at 500 hPa (Lhasa Workgroup for Tibetan Plateau Meteorology Research, 1981). In this study, a closed cyclonic circulation or cyclonic winds at 700 hPa over southwestern China is defined as an SWV.

According to the definitions of TPVs and SWVs, 18 TPVs and 18 SWVs whose locations at each time derived from the FNL data and the observational data are similar are selected in the May–August 2000–2011 period. Among these vortices, the genesis processes of nine SWVs were accompanied by moving-off TPVs, which are defined as Situation A. There are nine moving-off TPVs unaccompanied by the genesis of SWVs, which we define as Situation B. Situation C refers to nine SWVs generated in the absence of moving-off TPVs. Figure 2 shows the trajectories of the TPVs and SWVs under these three situations (The times and locations of the vortices in the three situations are provided as the supporting information in Table S1, S2, S3, respectively). In Figures 2(a) and (c) we can see that most of the SWVs are generated in the area 104–109°E, 28–35°N (the green box in Figure 2). Therefore, we refer to the area as the genesis region of SWVs (or 'genesis region' for short). By comparing the genesis process of SWVs in Situation A to those in Situation B and C, we will investigate the role played by the moving-off TPVs in the genesis process of SWVs.

In Situation A, in order to investigate the effect of moving-off TPVs on the genesis process of SWVs, the SWVs are selected to be those as they first appear on the synoptic map when the TPVs arrive at the eastern edge of the Tibetan Plateau around 103°E. Thus, we define the time of SWVs genesis as $t = 0$ in Situation A and C, and the time when the TPVs move off the Tibetan Plateau as $t = 0$ in Situation B to ensure the comparability in these three situations. The times 6, 12 and 18 h before $t = 0$ are taken as $t = -6$, $t = -12$, $t = -18$, and 6 and 12 h after as $t = +6$ and $t = +12$, with the units of hours, respectively. In the following text, the units are omitted for short to mark the time.

2.3. Composite method

To obtain the common genesis features of SWVs, we use the traditional composite method, which presents averaged features for all cases. Considering the moving features of TPVs, following the analysis used in previous research on typhoons (Frank, 1977; Gray, 1981; Li *et al*., 2004), we use a dynamic composite method to analyse the common features of the meteorological elements associated with the TPVs. The so-called 'dynamic composite

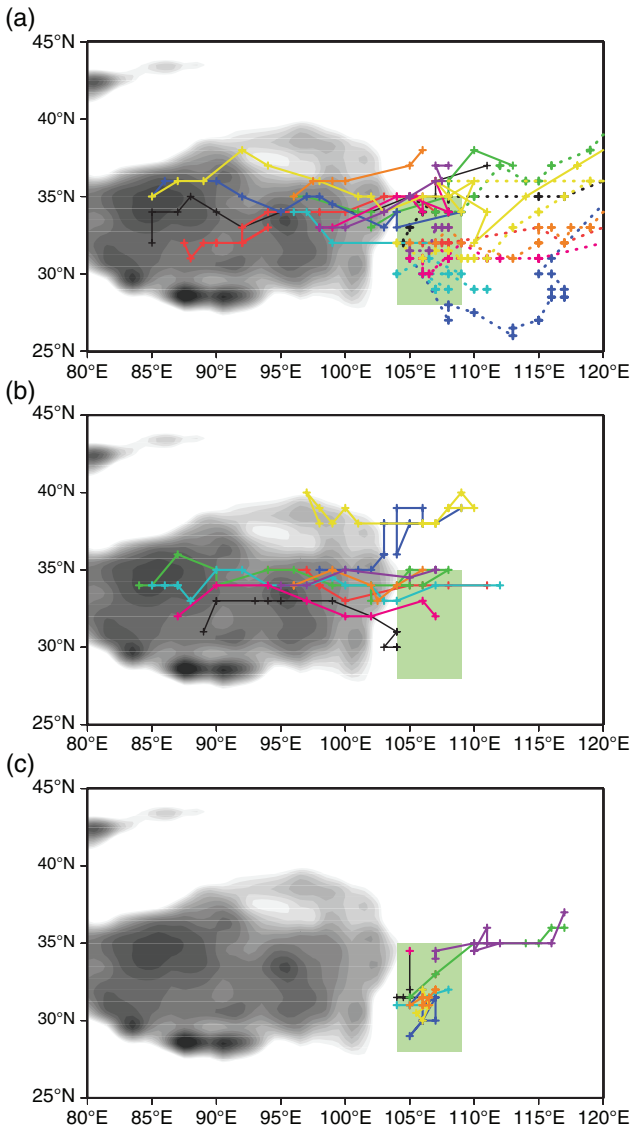

Figure 2. Trajectories of (a) nine SWVs accompanied by the moving-off TPVs (Situation A), (b) nine TPVs without genesis of SWVs (Situation B), and (c) nine SWVs without moving-off TPVs (Situation C). In (a) the trajectories of TPVs and SWVs are drawn in the same colour for each process, and the solid and dotted lines indicate the trajectories of TPVs and SWVs, respectively. The grey shading indicates terrain over 3000 m with the interval of 200 m, and the green box represents the genesis region (104–109°E, 28–35°N) of SWVs. The cross (+) in each track is the centre position of the vortex using a time interval of 6 h.

method' is to take the centre of the TPV concerned as the origin of coordinates, which moves along with the TPV, then to make a composite for every case in a same scope at each time in the moving coordinate system. Thus, the origin of the coordinates is the composite centre, and the coordinates represent the distances to the composite centre. The dynamic composite method has been used in the study of TPVs by Li *et al.* (2011, 2014a).

2.4. *Apparent heat source and apparent moisture sink*

To investigate the effect of the diabatic heating in the genesis process of SWVs, we calculate the atmospheric apparent heat source (Q_1) and the apparent moisture sink (Q_2) in the genesis region of SWVs based on the thermodynamic and moisture equations. The equations used are as follows (Yanai *et al.*, 1973):

$$Q_1 = c_p \left\{ \frac{\partial T}{\partial t} + \mathbf{V} \bullet \nabla T + \omega \left(\frac{P}{P_0} \right)^{\kappa} \frac{\partial \theta}{\partial p} \right\}, \tag{1}$$

$$Q_2 = -L \left(\frac{\partial q}{\partial t} + \mathbf{V} \bullet \nabla q + \omega \frac{\partial q}{\partial p} \right), \tag{2}$$

where T is the temperature, $\mathbf{V}$ and ω denote the horizontal wind vector and the vertical wind component in pressure coordinates, respectively. P_0 is the pressure of 1000 hPa, c_p represents the specific heat at constant pressure, and $\kappa \approx 0.286$. θ is the potential temperature. $L = 2.5 \times 10^6\ \mathrm{J\,kg^{-1}}$ denotes the latent heat of condensation, and q is the specific humidity. The vertically integrated forms of Eqs (1) and (2) can be written as follows:

$$< Q_1 > \approx LP + S + < Q_R >, \tag{3}$$

$$< Q_2 > \approx LP - LE, \tag{4}$$

where P, S and E represent the amount of precipitation, surface sensible heat flux, and eddy moisture flux, respectively, and $<Q_R>$ denotes radiative heating (cooling). Usually, in the precipitation process, S, $<Q_R>$ and LE are feeble compared with LP. Thus, similar values and distributions of Q_1 and Q_2 imply that LP (the condensation latent heat) is the major component of Q_1.

2.5. *Potential vorticity (PV) budget*

The Ertel potential vorticity (PV) equation (Hoskins *et al.*, 1985; Wu and Liu, 1999) is utilized to analyse the PV budget in the genesis region of SWVs. The PV tendency equation without frictional effects can be given as:

$$\frac{\mathrm{d}P_E}{\mathrm{d}t} = \alpha \boldsymbol{\zeta}_\mathbf{a} \bullet \nabla_3 Q, \tag{5}$$

where P_E represents Ertel PV, α is the specific volume, and $\boldsymbol{\zeta}_\mathbf{a} = (f\mathbf{k} + \nabla_3 \times \mathbf{V}_3)$ is the absolute vorticity with $\mathbf{k}$ and $\mathbf{V_3}$ denoting the unit vector in the z-direction and wind vector, respectively. Q is the diabatic heating rate. The PV in pressure coordinates is

$$P_E = -g(f + \zeta_p)\frac{\partial \theta}{\partial p} + g\left(\frac{\partial v}{\partial p}\frac{\partial \theta}{\partial x} - \frac{\partial u}{\partial p}\frac{\partial \theta}{\partial y} \right), \tag{6}$$

where θ is the potential temperature, f is the Coriolis parameter, u and v represent zonal and meridional winds respectively. After removing the small terms and coordinate transformations (Li *et al.*, 2011), Eq. (5) can be written as

$$\frac{\partial P_E}{\partial t} = -\frac{\partial u P_E}{\partial x} - \frac{\partial v P_E}{\partial y} - \frac{\partial \omega P_E}{\partial p} + g\frac{\partial v}{\partial p}\frac{\partial Q}{\partial x} - g\frac{\partial u}{\partial p}\frac{\partial Q}{\partial y} - g(f + \zeta_p)\frac{\partial Q}{\partial p}, \tag{7}$$

where $\zeta_p = \frac{\partial v}{\partial x} - \frac{\partial u}{\partial y}$ is the relative vorticity about a vertical axis. The first two terms on the right-hand side of Eq. (7) are the horizontal PV flux divergences. The third term is the vertical PV flux divergence. The fourth and fifth terms are related to redistribution of PV induced by the horizontally uneven distribution of Q, while the sixth term arises from the vertically uneven distribution of Q. Equation (7) indicates that contributions to the local PV change come from the horizontal and vertical PV flux divergences, as well as the PV redistributions due to the spatially uneven distribution of Q (Pan *et al.*, 2008). Previous studies (Li *et al.*, 2011, 2014a) have demonstrated that PV budget analysis is good at revealing the dynamic and thermodynamic features of TPVs.

3. Large-scale circulations in Situation A

3.1. *500 hPa*

Figure 3 shows the dynamic TPV-centred composites of geopotential height and winds at 500 hPa, and vorticity and locations of SWVs at 700 hPa in Situation A. From $t = -18$ to

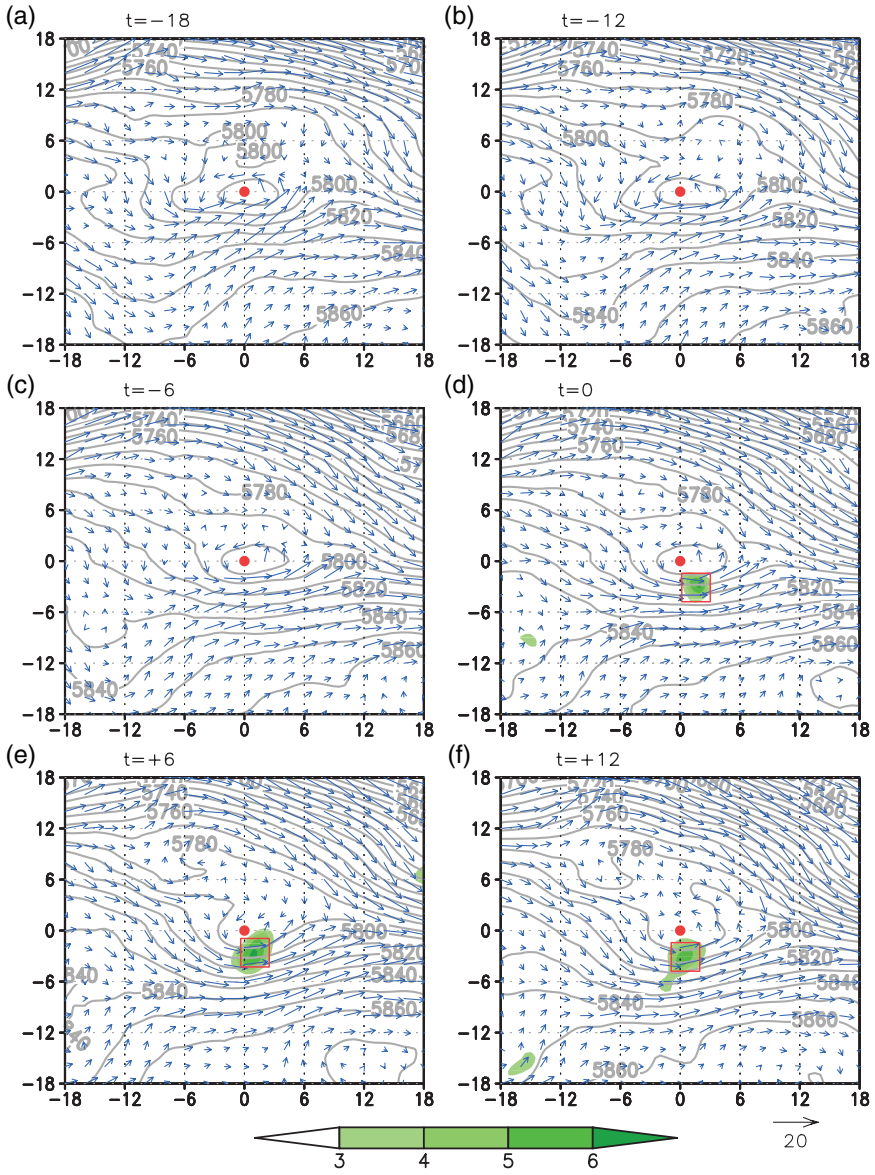

Figure 3. TPVs-centred dynamic composites of 500 hPa geopotential heights (grey contours; unit: gpm), winds (blue vectors; unit: m s^{-1}) and 700 hPa vorticity (shadings; unit: 10^{-5} s^{-1}) for nine cases in Situation A at (a) $t=-18$, (b) $t=-12$, (c) $t=-6$, (d) $t=0$, (e) $t=+6$, (f) $t=+12$ (unit: h). The red boxes indicate the locations of SWVs, and the red dots represent the centres of TPVs. The x- and y-axes are relative longitude and latitude, respectively.

$t=+12$, there are strong northerly winds in front of the ridge to the north of the Tibetan Plateau invading to the east of the TPVs. The southwesterly winds to the south of the TPVs converge with the northerlies to the east of the TPVs, benefiting for the rainfall there. The rainfall belt of the observed accumulated rainfall from $t=-18$ to $t=+12$ stretches from the eastern Tibetan Plateau to the middle Yangtze River Valley, with the centre located at the genesis region of the SWVs (figure not shown). Such convergence and the latent heat release associated with the precipitation are crucial for the eastward motion of TPVs (Li *et al.*, 2011, 2014a, 2017). Before the TPVs move off the Tibetan Plateau (Figures 3(a)–(c)), the southwesterlies are mainly from the Bay of Bengal (the ground-relative composites figures are not shown). After the TPVs move off the Tibetan Plateau, at $t=0$ and $t=+6$ (Figures 3(d) and (e)), the subtropical high located over southeastern China is enhanced, which strengthens the warm and humid monsoon southwesterlies and is favourable for the genesis and maintenance of SWVs. Thus, positive vorticity centres can be observed to the south of the TPVs in the SWV genesis region.

3.2. *700 hPa*

The dynamic composites of 700 hPa winds and wind speeds in Situation A are shown in Figure 4. Considering that the main body of the Tibetan Plateau is over 4000 m and higher than the level of 700 hPa, we remove the figures for $t=-18$ and $t=-12$ when the TPVs are still located over the Tibetan Plateau. It can be seen that when the TPVs are near the east edge of the Tibetan Plateau (Figure 4(a)), there are strong southwesterly winds and weak cyclonic shear to the southeast of the TPVs, providing favourable conditions for the genesis of SWVs. The southwesterly winds are strengthened after the TPVs move off the Tibetan Plateau (Figures 4(b) and (c)). The increased southerlies can transport more water vapour to the east and south of the TPVs and enhance the convergence, benefiting the genesis of the SWVs and rainfall over southwestern China. In fact, the appearance of SWVs occurs at the time when the TPVs are around the edge of the Tibetan Plateau ($t=0$) (Figure 4(b)).

4. Dynamic and thermodynamic features in the genesis of SWVs

4.1. *Structure of the circulations*

In order to investigate the evolution process of meteorological elements over the genesis region of SWVs, and reveal the effect of the TPVs on the circulation, the structures of the dynamic and thermodynamic factors in Situation A are given in Figure 5.

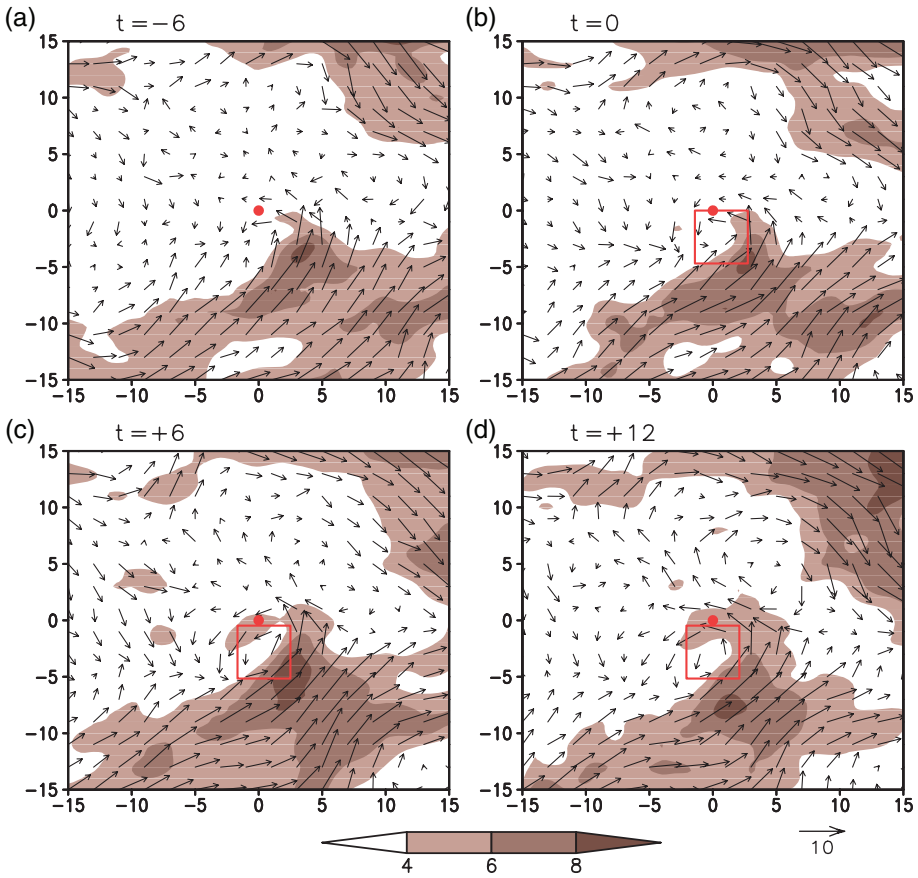

Figure 4. TPVs-centred dynamic composites of 700 hPa winds (vectors; unit: m s^{-1}) and wind speeds (shading unit: m s^{-1}) at (a) $t=-6$, (b) $t=0$, (c) $t=+6$, (d) $t=+12$ (unit: h) in Situation A. The red boxes indicate the locations of SWVs, and the red dots represent the centres of TPVs. The x- and y-axes are relative longitude and latitude, respectively.

It can be seen in Figure 3 that at 500 hPa the northerlies in front of the ridge to the northeast of the Tibetan Plateau and southwesterlies to the south of the TPVs converge to the east of the TPVs. As shown in Figure 5(a), at 500 hPa when the TPVs move eastward the vorticity and convergence over the genesis region strengthen, and at 700 hPa in the genesis region of SWVs there are weak positive vorticity and convergence before $t=0$, and they also strengthen gradually. With the eastward movement of the TPVs, the convergence associated with the TPVs at 500 hPa overlaps the convergence at lower levels, thus, convergence over the genesis region of SWVs enhances gradually from $t=-18$ to $t=0$ (Figure 5(a)). At upper levels, as the TPVs move off the Tibetan Plateau, at $t=0$ the intensity of the divergence over the genesis area is the strongest. Consequently, the upper-level divergence and low-level convergence are favourable for ascending motion over the genesis region, so strong and deep ascending motion is observed in Figure 5(a). In Figure 5(b), the contours of Q_1 and Q_2 are similar to each other, implying that condensational latent heat is the major component of the atmospheric heat source. It has been shown in Figure 4 that the southwesterlies at 700 hPa prevail to the south and east of the TPVs, which is favourable for transporting humid air from the south, and because of the remarkable ascending motion, may trigger heavy rainfall. As is well known, the upper-level latent heating associated with the rainfall can depress lower-level isobaric surfaces, benefiting the formation of SWVs at 700 hPa.

4.2. *Water vapour budget*

The net water vapour budget over the genesis region from $t=-18$ to $t=+12$, as well as the water vapour transported through the four boundaries at $t=-6$ and $t=0$ in Situation A are shown in Figures 6(a) and (b), respectively. The net water vapour budget over the genesis region increases gradually from $t=-18$ to $t=-6$, reaches the peak at $t=-6$ (Figure 6(a)) and then declines. As shown above, the SWVs generate at $t=0$, just after the water vapour budget reaches its maximum, indicating the importance of water vapour in the genesis of SWVs. In order to reveal the main source of the water vapour transported to the genesis region, we calculate the water vapour transported through the four boundaries at $t=-6$ and $t=0$ (Figure 6(b)). Obviously, the net inflow of the water vapour mainly comes through the south and west boundaries, and the inflow from the former is more abundant than that from the latter. Here we can see that the southerly winds have an important effect on the net water vapour budget over the genesis region, which is favourable for precipitation and corresponding latent heat release (Figure 5(b)).

5. Genesis mechanism of the SWVs

To discuss the generation mechanism of SWVs when accompanied by moving-off TPVs, we calculate the PV budget at 700 hPa at $t=-6$ and $t=0$ (Figure 7). The similar values and distribution of Q_1 and Q_2 in Figure 5(b) indicate that the condensational latent heat is the major component of the atmospheric heat source. Thus, we take the condensational latent heating rate $\dot{\theta}$ as Q to calculate PV tendency expressed by Eq. (7). According to Emanuel *et al.* (1987) and Raymond (1992), $\dot{\theta}$ can be expressed as

$$\dot{\theta} = \frac{\mathrm{d}\theta}{\mathrm{d}t} = \omega\left(\frac{\partial\theta}{\partial p} - \frac{\gamma_\mathrm{m}}{\gamma_\mathrm{d}}\frac{\theta}{\theta_\mathrm{e}}\frac{\partial\theta_\mathrm{e}}{\partial p}\right), \tag{8}$$

where γ_m and γ_d are the adiabatic lapse rates of moist and dry air, respectively. ω is the vertical wind component in pressure coordinates. θ and θ_e are potential temperature and pseudoequivalent potential temperature, respectively.

At $t=-6$ and $t=0$, there are positive PV tendencies over the genesis region (Figures 7(a) and (e)), indicating the development of the cyclonic circulation at 700 hPa. In the eastward-moving

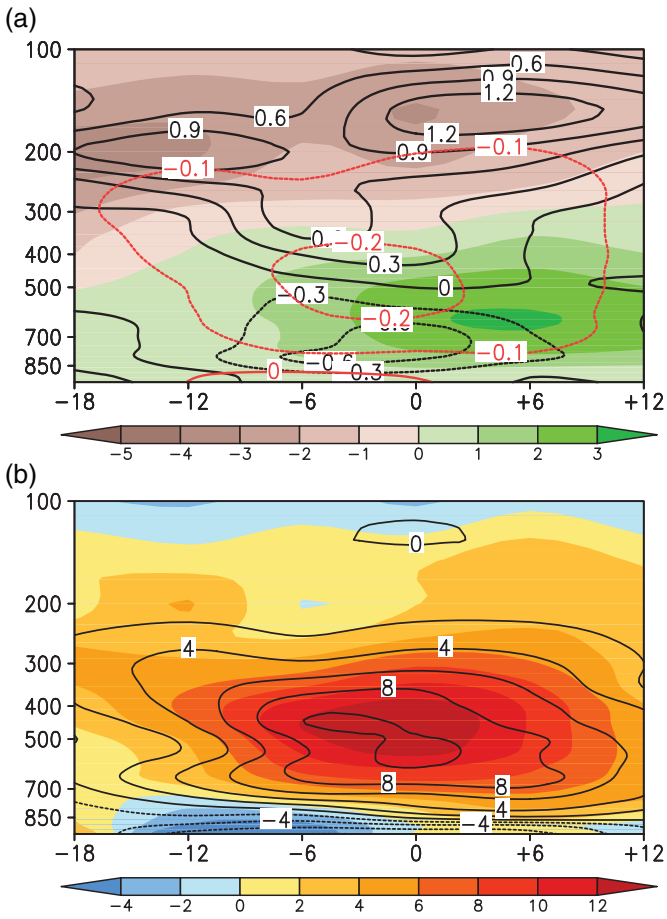

Figure 5. The height–time cross-sections of (a) vorticity (shading; unit: $10^{-5}\,s^{-1}$), divergence (black contours; unit: $10^{-5}\,s^{-1}$), vertical velocity (red contours; unit: $Pa\,s^{-1}$), and (b) Q_1 (shading; unit: $K\,day^{-1}$) and Q_2 (black contours; unit: $K\,day^{-1}$) averaged over the genesis region of SWVs (104–109°E, 28–35°N) in Situation A.

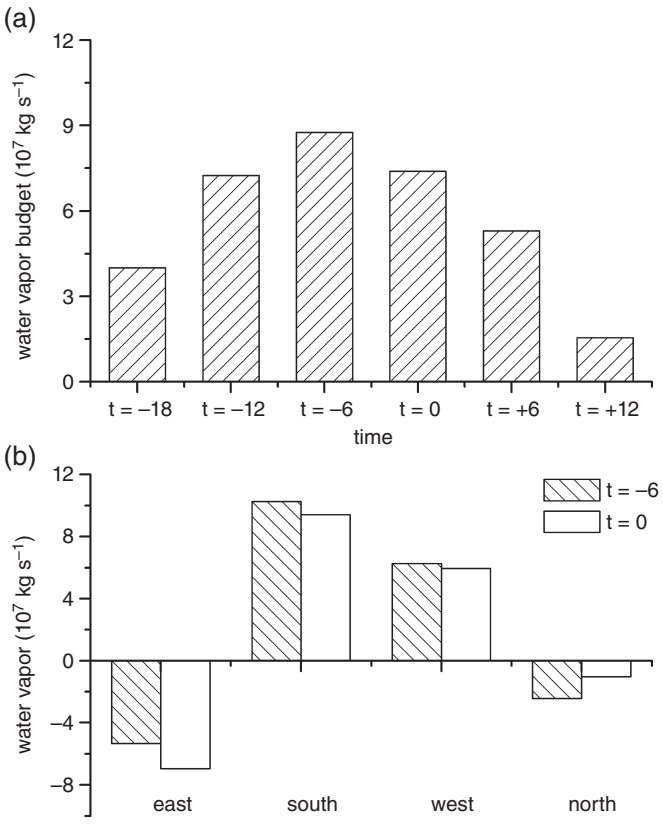

Figure 6. (a) Net water vapour budget (unit: $10^7\,kg\,s^{-1}$) over the genesis region of SWVs, and (b) the vertically integrated water vapour transported through its four boundaries at $t=-6$ and $t=0$ (unit: $10^7\,kg\,s^{-1}$) in Situation A.

process of TPVs, the convergence at 700 hPa and the ascending motion become stronger, and the maxima are found at $t=0$ (Figure 5(a)). Thus, the positive contribution from horizontal PV flux divergence ($-\frac{\partial uP_E}{\partial x}-\frac{\partial vP_E}{\partial y}>0$) is over most of the genesis region at $t=0$, with the maximum located to the northeast of the centres of SWVs (Figure 7(f)). Simultaneously, the notable updraught is conducive to vertical PV divergence, so the vertical PV flux divergence term has a negative effect ($-\frac{\partial \omega P_E}{\partial p}<0$) on the generation of SWVs (Figures 7(c) and (g)). The net water vapour budget increases from $t=-18$ to $t=-6$, and reaches its peak at $t=-6$ (Figure 6(a)). Abundant water vapour is lifted due to the strong convergence and updraught over the genesis region, leading to latent heat release (Figure 5(b)). The latent heating depresses the isobaric surface in the lower troposphere and strengthens the low-level cyclonic disturbance, which is favourable for the generation of SWVs ($-g(f+\zeta_p)\frac{\partial Q}{\partial p}>0$, $g\frac{\partial v}{\partial p}\frac{\partial Q}{\partial x}-g\frac{\partial u}{\partial p}\frac{\partial Q}{\partial y}$ is faint and negligible). Consequently, the latent heating associated with the precipitation is the most important factor promoting the generation of SWVs (Figures 7(d) and (h)).

The results derived from the calculations on 700 hPa are also found on the other levels around 700 hPa, and the maxima of the contribution from latent heating appear at 700 hPa (figure not shown), where the SWVs are generated.

6. Effect of TPVs

The latent heat associated with precipitation is closely related to the lower-level convergence and the water vapour budget. From Figure 6(b) we have seen that the water vapour transported through the southern boundary of the genesis region is most significant. Then, it seems that the southerlies are also an important factor influencing the genesis of SWVs.

6.1. *Southerly winds and water vapour in Situations A and B*

In order to compare the southerlies over the genesis region to those when the TPVs move off the Tibetan Plateau but no SWVs are generated (Situation B), Figure 8 shows composites of the meridional winds at 700 hPa averaged between 104°E and 109°E from $t=-18$ to $t=+12$ for Situations A and B, respectively. The southerlies control most of the genesis region in both situations, but the wind speeds in Situation A are greater than those in Situation B to the south of 34°N. In Situation A (Figure 8(a)), the southerly winds strengthen from $t=-18$ to $t=-6$, and reach a peak at $t=-6$, coinciding with the water vapour budget in Figure 6(a). This illustrates the important role of the southerly winds in transporting the water vapour. Besides, the value of the southerly winds in Situation A is about three times larger than that in Situation B at $t=0$. The intensity of the southerlies in situation B reaches the maximum at $t=-6$, and then reduces (Figure 8(b)). Correspondingly, the water vapour is mainly transported through the western boundary (Figure 9(b)), and the net water vapour budget decreases from $t=-12$ to $t=+12$ (Figure 9(a)). It is worth mentioning that the value of the water vapour inflow through the western boundary in Situation B is similar to that in Situation A. Therefore, the difference of the southerlies between these two situations results in the different water vapour budget in the genesis region, indicating that the southerly winds are the fundamental factor in the genesis of the SWVs.

6.2. *Southerly winds and water vapour in Situation C*

To further discuss the effect of TPVs on the genesis of the SWVs, nine SWVs cases which were not accompanied by moving-off TPVs are chosen.

The southerly wind speed, net water vapour budget over the genesis area of SWVs as well as the water vapour transported

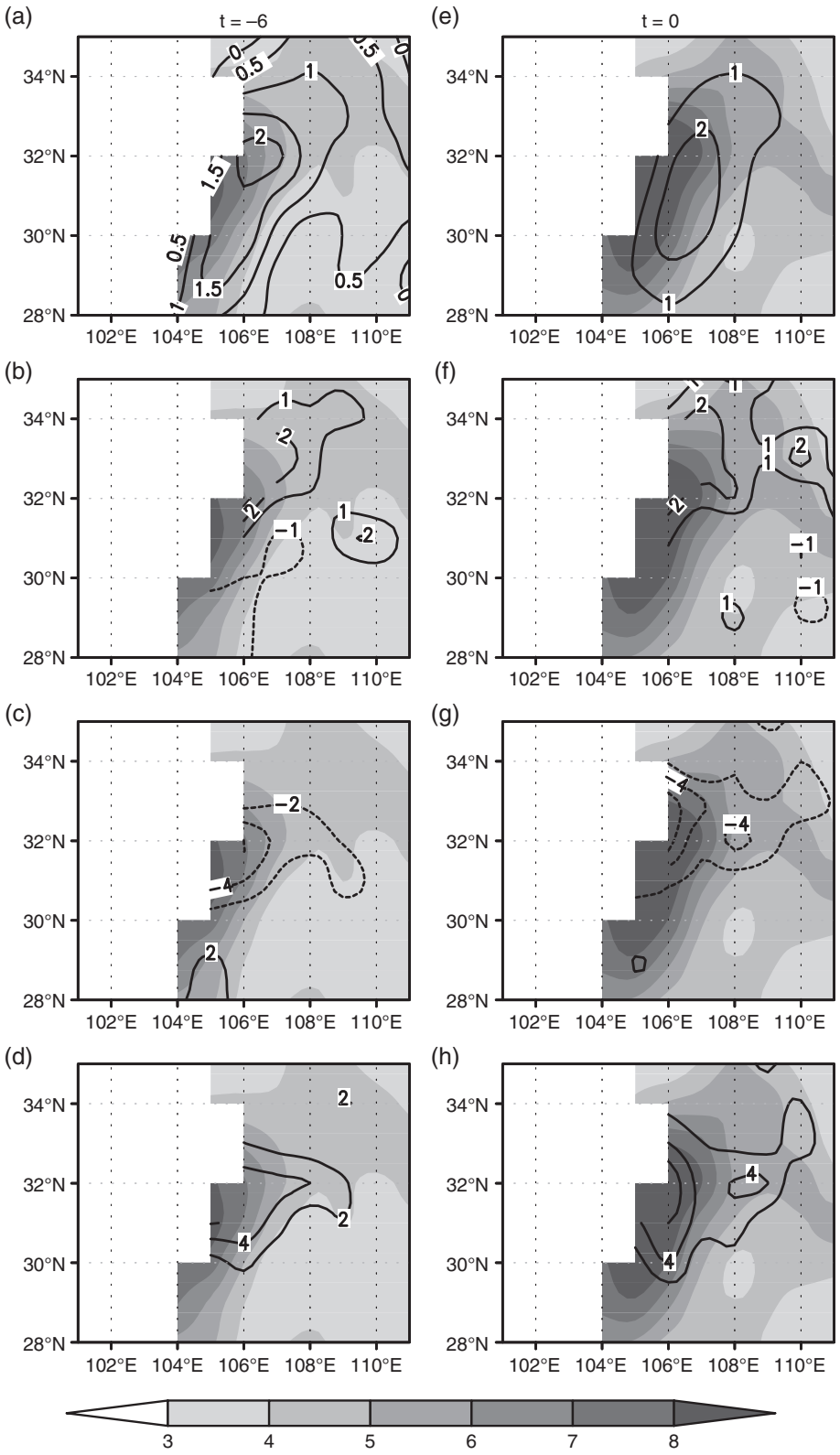

Figure 7. PV budgets in Situation A in the genesis region at 700 hPa (contours; unit: PVU $(6\,\mathrm{h})^{-1}$, $1\,\mathrm{PVU} = 10^{-6}\,\mathrm{m^2\,s^{-1}\,K\,kg^{-1}}$) and 700 hPa PV (shadings; unit: PVU) at (a–d) $t = -6$ and (e–h) $t = 0$. The panels from the uppermost to the lowest are (a) and (e) the tendency, (b) and (f) the horizontal PV flux divergence, (c) and (g) the vertical PV flux divergence, (d) and (h) the effect of the condensation latent heat.

through its four boundaries for Situation C are presented in Figures 10 and 11, respectively. The maximum of southerly winds speed in Situation C is similar to that in Situation A. However, the wind speed increases greatly from $t = -18$ to $t = -6$ for the latter (Figure 8(a)), while its variation from $t = -18$ to $t = -6$ for the former is small (Figure 10). In fact, the obvious enhancement of the southerlies can also be seen in Situation B (Figure 8(b)), but is weaker than that in Situation A, demonstrating that the eastward-moving TPVs have a relationship with the southerly winds over the genesis region. Although the intensity of the southerlies is almost the same at $t = -6$ in Situations C and A, the net water vapour budget in Situation C is significantly less than that in Situation A (Figures 6(a) and 11(a)). In Situation C, water vapour is transported to the genesis region of SWVs through the southern boundary, and out of the region through the eastern boundary (Figure 11(b)), implying weak convergence of the water vapour over the genesis region of the SWVs. Thus, the moving-off TPVs tend to intensify the convergence field. To further reveal the effect from the TPVs on the meteorological element fields over the genesis region of the SWVs, we discuss

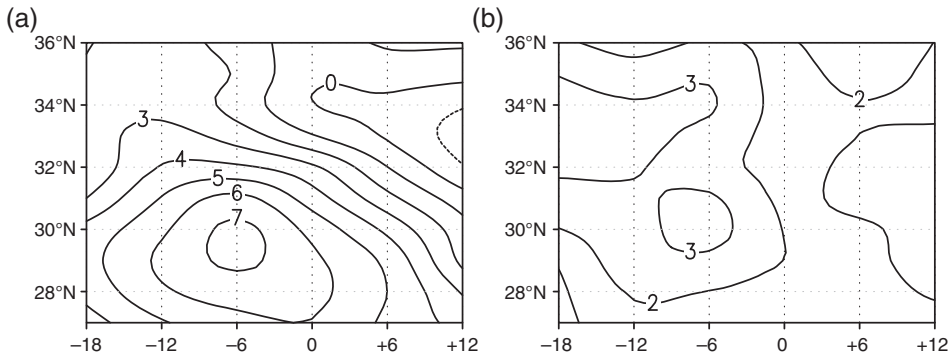

Figure 8. Time–latitude cross-sections of southerly wind speeds (unit: m s^{-1}) averaged between 104°E and 109°E in (a) Situation A and (b) Situation B. The *x*-axis denotes time with units of hours.

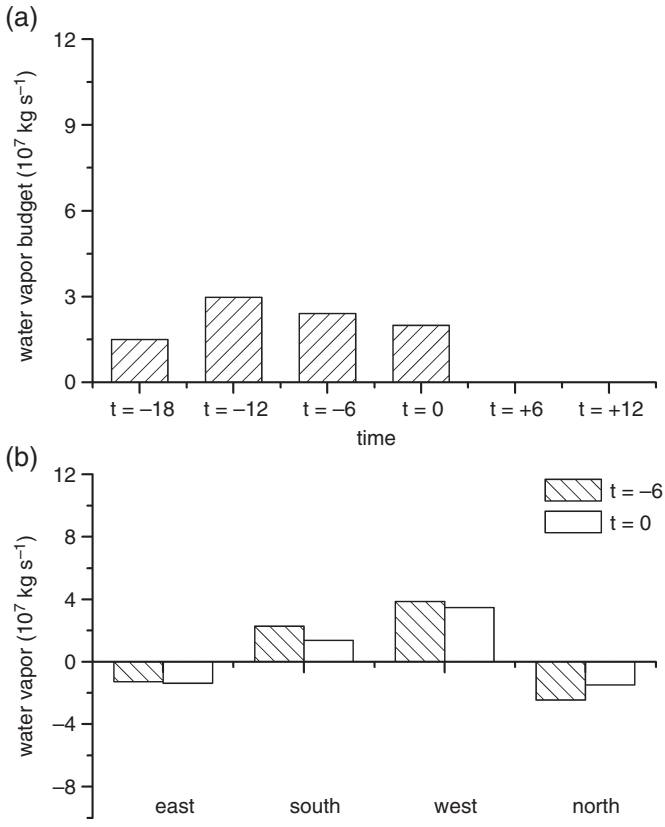

Figure 9. (a, b) Same as Figure 6 but for Situation B.

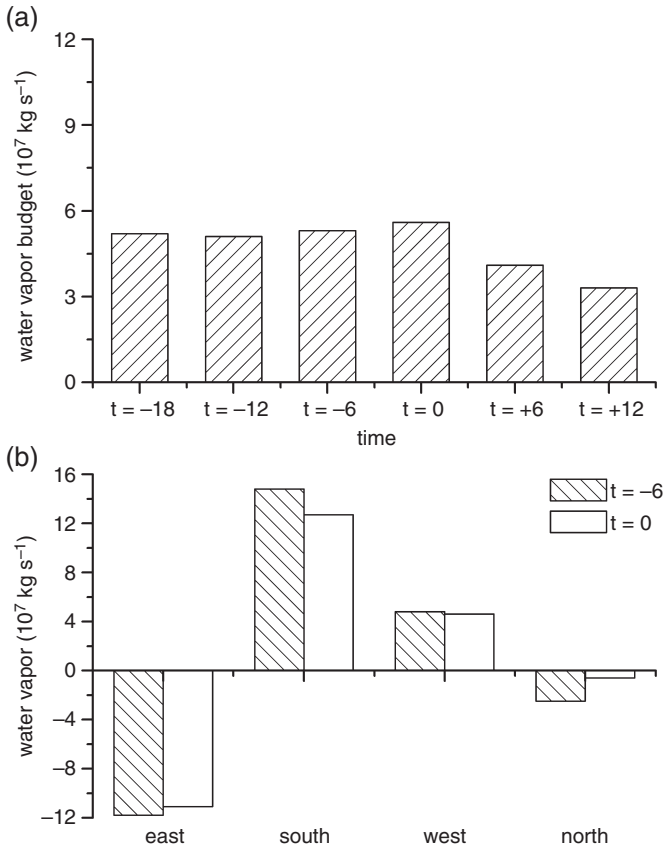

Figure 11. (a, b) Same as Figure 6 but for Situation C.

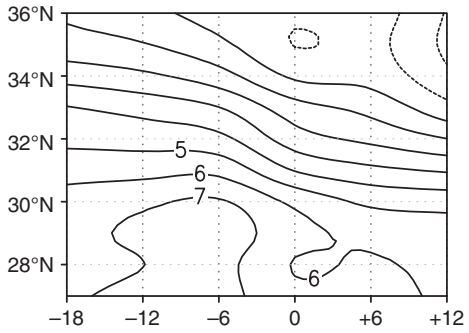

Figure 10. Same as Figure 8 but for Situation C.

the structure of the circulations in Situation C in the next subsection.

6.3. *Structure of the circulations in Situation C*

Height–time cross-sections of the composites for vorticity, divergence, vertical velocity, as well as Q_1 and Q_2 averaged over the genesis region in Situation C are shown in Figure 12, and the differences between Situations A and C are shown in Figure 13. In Situation C, the positive vorticity and convergence are very shallow, with the former located below about 400 hPa while the latter is below 700 hPa (Figure 12(a)). Moreover, the ascending motion is very weak (Figure 12(a)). From Figures 13(a) and (b), it can be seen that the TPVs seem to weaken the positive vorticity and convergence at lower levels in the genesis region before they move off the Tibetan Plateau ($t = 0$) in Situation A, and the cyclonic vorticity and the convergence are weaker compared with those in Situation C, which may be induced by the sinking flow of the TPVs' circulation to the east of the TPVs (Chen *et al.*, 2004; Xiao *et al.*, 2009; Zhou *et al.*, 2009), as can be seen in Figure 13(c). However, the negative effect from the TPVs attenuates with time; the status changes when the TPVs are near to the edge of the Tibetan Plateau (between $t = -6$ and $t = 0$). Then the TPVs strengthen and enhance the positive vorticity and convergence fields when they move off and arrive at the genesis region ($t = 0$); at this time, the convergence and ascending motion are deeper and stronger than those at previous times and than in Situation C. Moreover, the differences shown

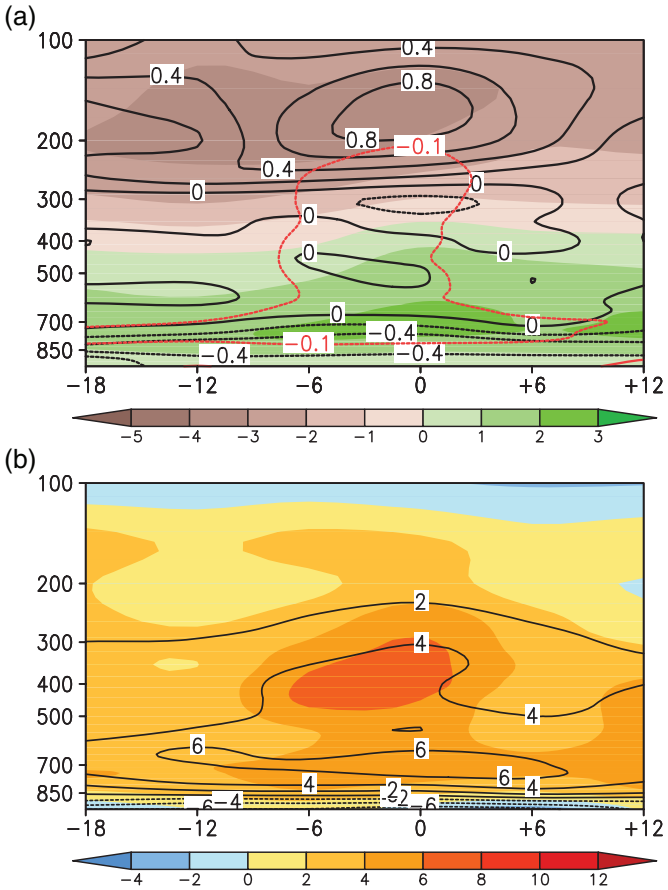

Figure 12. (a, b) Same as Figure 5 but for Situation C.

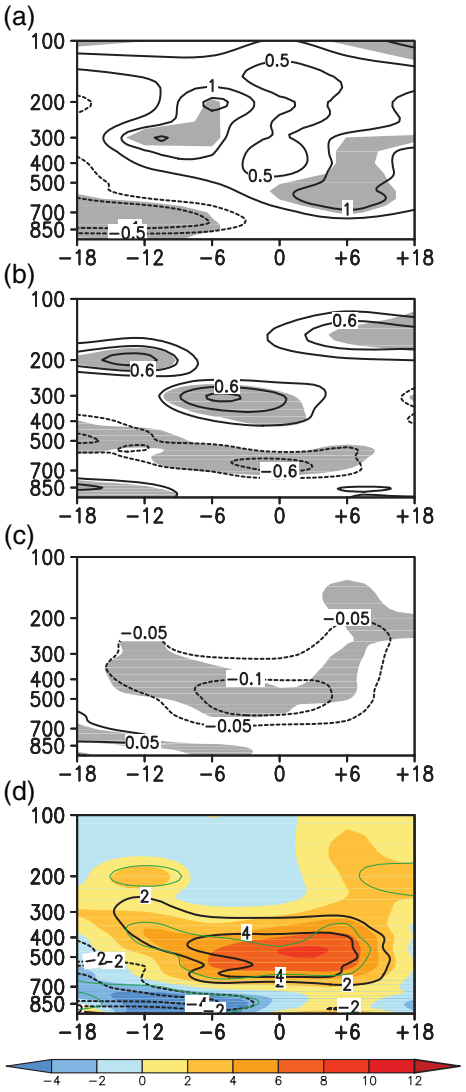

Figure 13. Differences of (a) vorticity (unit: $10^{-5}\,s^{-1}$), (b) divergence (unit: $10^{-5}\,s^{-1}$), (c) vertical velocity (unit: $Pa\,s^{-1}$), and (d) Q_1 and Q_2 (unit: $K\,day^{-1}$) between Situations A and C. The grey shadings in (a), (b), (c) and the areas enclosed in the green lines in (d) indicate where significance exceeds the 90% confidence level using a *t*-test. In (d) the significance contour is shown for Q_1 only.

in Figure 13 have a similar pattern with the structure of the three factors (vorticity, divergence and ascending velocity) in Situation B (figure not shown), further verifying the effect from the TPVs. Thus, the circulations in Situation A are more favourable for intensifying the convergence and ascending motion, leading to heavier precipitation and increased latent heating over the genesis region, beneficial for the genesis of SWVs (Figure 13(d)).

The vorticity, divergence, vertical motion, Q_1 and Q_2 averaged between 500 and 700 hPa over the genesis region of SWVs are calculated in Situations A and C, respectively, and the brief results of the difference between Situations A and C are shown in Table 1. Obviously, the convergence, ascending motion and heating fields are much stronger in Situation A than those in Situation C at both $t = 0$ and $t = +6$, indicating favourable conditions for the generation of SWVs in the former. In fact , at $t = 0$, the average intensity of the SWVs in Situation A is $0.3 \times 10^{-5}\,s^{-1}$ larger than that in Situation C, while at $t = +6$ the value is $1.65 \times 10^{-5}\,s^{-1}$. Besides, in Situation A, there are eight SWVs lasting over 48 h, and only four in Situation C. Therefore, the conditions associated with the TPVs are more beneficial for the genesis of SWVs, and even their survival time.

7. Conclusions and discussion

SWVs are important rain-producing systems in southwestern China, which can trigger heavy rainfall, even flood disasters, over wider areas in eastern China when they move eastward. The study of the genesis mechanism of SWVs is important not only in understanding the SWVs themselves, but also in forecasting the precipitation over southwestern and even eastern China. TPVs are mesoscale systems forming over the Tibetan Plateau; they always exert an important effect on genesis and development of the SWVs when they move off the Tibetan Plateau. Previous studies mainly focused on the relations of the moving-off TPVs to the pre-existing SWVs, and only a few studies discussed the effects of TPVs on the genesis of SWVs, but considered just one case. Besides, contradictory results are obtained from numerical models. The present work compared three situations which include nine cases, respectively, by reanalysis data diagnosis, which is more comprehensive and solid, to investigate the role played by TPVs in the genesis process of SWVs.

In this study, the generation mechanism of SWVs is accompanied by the TPVs moving off the Tibetan Plateau, and the key factors in the generation process are analysed in Situation A, revealing the dominant effect of the condensational latent heat in the genesis of SWVs. Furthermore, the effect of TPVs is discussed by comparing to situation of moving-off TPVs that are not associated with genesis of SWVs (Situation B) and the genesis process without the moving-off TPVs (Situation C). The results are summarized as follows.

Along with the eastward movement of the TPVs, at 500 hPa there is a ridge to the northeast of the TPVs from $t = -18$ to $t = +12$, and the northerly winds in front of the ridge converge with the southwesterlies intensively to the east of the TPVs. The 700 hPa southwesterly winds to the south of the TPVs have an important effect on the genesis of SWVs. The net water vapour budget over the genesis region suggests that water vapour is mainly transported through the southern boundary. The positive vorticity advection and convergence at 500 hPa are covering the genesis region as the TPVs move eastward, intensifying the ascending motion there. At the time when the TPVs move

Table 1. Vorticity (unit: 10^{-5} s^{-1}), divergence (unit: 10^{-5} s^{-1}), vertical motion (unit: Pa s^{-1}), Q_1 (unit: K day^{-1}) and Q_2 (unit: K day^{-1}) averaged between 500 and 700 hPa over the genesis region of SWVs.

Time	Vorticity (10^{-5} s^{-1})	Divergence (10^{-5} s^{-1})	Vertical motion (Pa s^{-1})	Q_1 (K day^{-1})	Q_2 (K day^{-1})
$t=0$	0.68	−0.41	−0.08	5.04	3.24
$t=+6$	1.08	−0.33	−0.06	4.85	3.4

off the Tibetan Plateau, the upper-level divergence and low-level convergence, as well as the latent heat release caused by convergent ascending motion, are favourable for the genesis of SWVs.

The structure of the meteorological features over the genesis region in Situation A shows that convergence, positive vorticity and ascending motion strengthen as the TPVs move eastward. To reveal the mechanism and the fundamental factors in the genesis process of SWVs, the PV budget in Situation A is calculated. The results show that the condensational latent heat and the horizontal PV flux convergence make a positive contribution to the genesis of SWVs, and the former is more important. The southerlies are an important factor in promoting the genesis of the SWVs, which are conducive to the convergence at lower levels and important in the water vapour transport over the genesis region. Moreover, by comparing Situation B with Situation A, the role of the southerlies is verified, indicating that the SWVs will not be generated without strong southerlies even under the effect of the moving-off TPVs. The water vapour transport associated with the southerlies is a vital factor in the generation of SWVs.

In order to further understand the effect of the moving-off TPVs, Situation C is compared with Situation A. The convergence, vorticity and ascending motion are significantly stronger and deeper when the TPVs move off the Tibetan Plateau in Situation A, indicating that TPVs strongly strengthen and deepen the vorticity, convergence fields and ascending motion. In fact, the SWVs in Situation A are much stronger and survive longer than those in Situation C. Therefore, the conditions associated with the TPVs are more beneficial for the genesis of SWVs, and even their survival time. It should be noted that in Situation A the positive vorticity and convergence at lower levels are weaker before the TPVs move off the Tibetan Plateau compared to those in Situation C, which may be induced by the sinking flow of the TPVs' circulation to the east of the TPVs.

All in all, moving-off TPVs are favourable for the generation of SWVs, and the SWVs are much stronger under the influence of the TPVs than those unaccompanied by the TPVs. However, SWVs may not be generated just under the action of the TPVs, since the water vapour transport associated with southerlies is another prominent factor affecting the genesis of SWVs. However, it should be pointed out that the intensity of TPVs in Situations A and B are different, which may have some relationship to the generation of SWVs in Situation A but not in Situation B. Therefore, which is more dominant in the genesis processes of SWVs: the southerly winds and the associated water vapour budget or the TPVs? This may be resolved by numerical experiments in future studies.

Acknowledgements

The authors are very grateful for the constructive comments from the associate editor and anonymous reviewers. The observational data are provided by the Information Center of Chinese Academy of Meteorological Sciences (CAMS). This work was supported by National Key Research and Development Program (Nos. 2016YFA0601504, 2016YFA0600602), the National Natural Science Foundation of China (Grant Nos. 41405054, 41221064 and 41275050), the National Key Basic Research and Development Program (No. 2012CB417205), the Basic Scientific Research and Operation Foundation of the CAMS (Nos. 2015Z001, 2016Y001), and the Special Fund for Tibetan Plateau Research (GYHY201406001).

Supporting information

The following supporting information is available as part of the online article:
Table S1. Situation A.
Table S2. Situation B.
Table S3. Situation C.

References

Chen GX, He GB. 2008. The observed facts analysis of southwest vortex from 2000–2007. *Plateau Mountain Meteorol. Res.* **28**: 59–65.
Chen ZM, Xu ML, Min WB, Miu Q. 2003. Relationship between abnormal activities of southwest vortex and heavy rain the upper reach of Yangtze River during summer of 1998. *Plateau Meteorol.* **22**: 162–167.
Chen ZM, Min WB, Miu Q, He GB. 2004. A case study on coupling interaction between Plateau and southwest vortexes. *Plateau Meteorol.* **23**: 75–80.
Emanuel KA, Fantini M, Thorpe AJ. 1987. Baroclinic instability in an environment of small stability to slantwise moist convection. Part I: Two-dimensional models. *J. Atmos. Sci.* **44**: 1559–1587.
Frank WM. 1977. The structure and energetics of the tropical cyclone. I. Storm structure. *Mon. Weather Rev.* **105**: 1119–1135.
Fu SM, Sun JH, Zhao SX, Li WL, Li B. 2011. A study of the impacts of the eastward propagation of convective cloud systems over the Tibetan Plateau on the rainfall of the Yangtze-Huai River basin. *Acta Meteorol. Sin.* **69**: 581–600.
Gray WM. 1981. *Recent Advances in Tropical Cyclone Research from Rawinsonde Composite Analysis*. WMO Program on Research in Tropical Meteorology, World Meteorological Organization: Geneva, Switzerland.
Hoskins BJ, McIntyre ME, Robertson AW. 1985. On the use and significance of isentropic potential vorticity maps. *Q. J. R. Meteorol. Soc.* **111**: 877–946.
Kuo YH, Cheng LS, Anthe RA. 1986. Mesoscale analyses of the Sichuan flood catastrophe, 11–15 July 1981. *Mon. Weather Rev.* **114**: 1984–2003.
Kuo YH, Cheng LS, Bao JW. 1988. Numerical simulation of the 1981 Sichuan flood. Part I: Evolution of a mesoscale southwest vortex. *Mon. Weather Rev.* **116**: 2481–2504.
Lhasa Workgroup for Tibetan Plateau Meteorology Research. 1981. *Research of 500 hPa Vortices and Shear Lines Over the Tibetan Plateau in Summer*. Science Press: Beijing.
Li GP. 2002. *The Tibetan Plateau Dynamic Meteorology*. China Meteorological Press: Beijing.
Li L, Zhang RH, Wen M. 2011. Diagnostic analysis of the evolution mechanism for vortices over the Tibetan Plateau in June 2008. *Adv. Atmos. Sci.* **28**: 797–808.
Li L, Zhang RH, Wen M, Liu LK. 2014a. Effect of the atmospheric heat source on the development and eastward movement of the Tibetan Plateau vortices. *Tellus A* **66**: 24451. https://doi.org/10.3402/tellusa.v66.24451.
Li L, Zhang RH, Wen M. 2014b. Diurnal variation in the occurrence frequency of the Tibetan Plateau vortices. *Meteorol. Atmos. Phys.* **125**: 135–144.
Li L, Zhang RH, Wen M, Lü JM. 2017. Effect of the atmospheric quasi-biweekly oscillation on the vortices moving off the Tibetan Plateau. *Clim. Dyn.* https://doi.org/10.1007/s00382-017-3672-3.
Li Y, Chen LS, Wang JZ. 2004. The diagnostic analysis on the characteristics of large scale circulation corresponding to the sustaining and decaying of tropical cyclone after its landfall. *Acta Meteorol. Sin.* **62**: 167–197.
Lu JH. 1986. *Introduction to the Southwest Vortex*. China Meteorological Press: Beijing.
Luo SW. 1992. *Study on some Kinds of Weather Systems Over and Around the Qinghai-Xizang Plateau*. China Meteorological Press: Beijing.
Luo SW, He ML, Liu XD. 1994. Study on the vortex of the Qinghai-Xizang (Tibet) Plateau in summer. *Sci. China Ser. B.* **37**: 601–612.
Pan Y, Yu RC, Li J, Xu YP. 2008. A case study on the role of water vapor from southwest China in downstream heavy rainfall. *Adv. Atmos. Sci.* **25**: 563–576.
Qiao QM, Zhang YG. 1994. *Synoptic Meteorology of the Tibetan Plateau and its Effect on the Near Areas*. China Meteorological Press: Beijing.
Raymond DJ. 1992. Nonlinear balance and potential-vorticity thinking at large Rossby number. *Q. J. R. Meteorol. Soc.* **118**: 987–1015.
Tao SY. 1980. *Torrential Rain in China*. Science Press: Beijing.

Tao SY, Ding YH. 1981. Observational evidence of the influence of the Qinghai-Xizang (Tibet) Plateau on the occurrence of heavy rain and severe convective storms in China. *Bull. Am. Meteorol. Soc.* **62**: 23–30.

Wang B, Orlanski I. 1987. Study of a heavy rain vortex formed over the eastern flank of the Tibetan Plateau. *Mon. Weather Rev.* **115**: 1370–1393.

Wang W, Kuo YH, Warner TT. 1993. A diabatically driven mesoscale vortex in the lee of the Tibetan Plateau. *Mon. Weather Rev.* **121**: 2542–2561.

Wang X, Li YQ, Yu SH, Jiang XW. 2009. Statistical study on the plateau low vortex activities. *Plateau Meteorol.* **28**: 64–71.

Wu GX, Liu HZ. 1999. Complete form of vertical vorticity tendency equation and slantwise vorticity development. *Acta Meteorol. Sin.* **57**: 1–15.

Xiao HR, Gu QY, He GB, Wang J. 2009. Mechanism of the interaction between Plateau vortex and southwest vortex during a heavy rain event. *Torrential Rain Disasters* **28**: 14–20.

Yanai M, Steven E, Chu JH. 1973. Determination of bulk properties of tropical cloud clusters from large-scale heat and moisture budgets. *J. Atmos. Sci.* **30**: 611–627.

Ye DZ, Gao YX. 1979. *The Tibetan Plateau Meteorology*. Science Press: Beijing.

Zhang PF, Li GP, Fu XH, Liu YM, Li LF. 2014. Clustering of Tibetan Plateau vortices by 10–30-day intraseasonal oscillation. *Mon. Weather Rev.* **142**: 290–300.

Zhou CH, Gu QY, He GB. 2009. Diagnostic analysis of vorticity in a heavy rain event under interaction of Plateau vortex and southwest vortex. *Meteorol. Sci. Technol.* **37**: 538–544.

